PRODUCTION OF $\pi^{\pm}$, $K^{\pm}$, p, K^0 and Λ^0 IN HADRONIC Z^0 DECAYS*

The SLD Collaboration**

Stanford Linear Accelerator Center

Stanford University, Stanford, CA 94309

ABSTRACT

We have measured production rates and spectra of $\pi^{\pm}$, $K^{\pm}$, $p/\bar{p}$, K^0 and $\Lambda^0/\bar{\Lambda}^0$ in light- and heavy-flavor hadronic Z^0 decays and for particles and antiparticles separately in quark jets. The SLD Cherenkov Ring Imaging Detector was used to identify charged hadrons. Samples enriched in light (uds) and b events were tagged using impact parameters of charged tracks, and a sample enriched in quark (over antiquark) jets was tagged using the electron beam polarization. We observe a clear flavor dependence in production rates and spectrum shapes, but only a small effect in $\xi = \ln(1/x_p)$ peak positions. Differences between baryon and antibaryon spectra in quark jets offer direct confirmation that faster particles are more likely to contain the initial quark.

1 Introduction

The production of final state hadrons from initial hard partons, e.g. the quark and antiquark in $e^+e^- \to Z^0 \to q\bar{q}$, is currently believed to proceed in three stages. The first stage involves the radiation of gluons from the primary quark and antiquark, which in turn radiate gluons or split into $q\bar{q}$ pairs until their virtuality approaches the hadron mass scale. Such a "parton shower" is calculable in perturbative QCD, for example in the Modified Leading Logarithm Approximation [1]. The next stage, in which these soft partons turn into "primary" hadrons, is not understood quantitatively, although several hadronization models exist. The ansatz of Local Parton-Hadron Duality (LPHD) [1], namely that the distribution for a given hadron species is directly proportional to the parton distribution at some appropriate virtuality, allows the prediction of the shapes of primary hadron momentum spectra, and of the energy- and mass-dependences of their peaks.

The third stage, in which unstable primary hadrons decay into final state hadrons, complicates the interpretation of inclusive measurements. It is desirable to remove the effects of these decays when comparing with the predictions of QCD+LPHD. Additional complications arise in jets initiated by heavy quarks in which the leading heavy hadrons carry a large fraction of the beam energy, restricting that available to other primary particles, and then decay into a number of secondary particles.

Measurements of the production rates and spectra of identified particles are useful for constraining models and testing the predictions of QCD+LPHD. Several such measurements have been reported in e^+e^- annihilation and QCD+LPHD has been successful in describing the shape and energy dependence of inclusive momentum spectra as well as those of identified charged and neutral hadrons [2]. At a given CM energy W, the spectrum for identified pions peaks at a higher value of $\xi = \ln(W/2p)$, where p is particle momentum, than the spectra of higher mass particle types; however little mass dependence is observed between these other species. The use of the JET-SET hadronization model to correct for the effect of primary hadron decays has been

shown [3] to introduce a mass dependence; direct observation of this effect is desirable.

Previous measurements have used samples of jets initiated by equal numbers of primary quarks and antiquarks. Comparison of the spectrum of a given particle with that of its antiparticle in a pure sample of quark jets would provide additional information on the hadronization process. Baryons are particularly useful for this as a baryon can contain a primary quark but an antibaryon cannot.

In this paper we present an analysis of $\pi^\pm$, $K^\pm$, $p/\bar{p}$, K^0, and $\Lambda^0/\bar{\Lambda}^0$ production in hadronic Z^0 decays collected by the SLC Large Detector (SLD). The analysis is based upon the approximately 150,000 hadronic events obtained in runs of the SLAC Linear Collider (SLC) between 1993 and 1995. We measure production rates and momentum spectra in a "global" sample of all hadronic events and also in high-purity samples of "light" ($Z^0 \rightarrow u\bar{u}, d\bar{d}, s\bar{s}$) and "b" ($Z^0 \rightarrow b\bar{b}$) events. The light sample is largely free from effects of heavy quark production and decay, but contains decay products of other unstable primary hadrons. In addition we compare the baryon (p and Λ) spectra with those of their antiparticles in a high-purity sample of quark jets, selected using the large production asymmetry in polar angle induced by the SLC electron beam polarization.

2   The SLD and Hadronic Event Selection

This analysis of data from the SLD multi-purpose detector [4] used charged tracks measured in the Central Drift Chamber (CDC) [5] and silicon Vertex Detector (VXD) [6]. The CDC consists of 80 layers of axial or stereo sense wires in a uniform axial magnetic field of 0.6 T. The VXD is composed of CCDs containing a total of 120 million 22×22 μm pixels arranged in four concentric layers of radius between 2.9 and 4.2 cm. Including the uncertainty on the primary interaction point (IP), the CDC and VXD give a combined impact parameter resolution of $11\oplus76/(p_\perp\sqrt{\sin\theta})$ μm, where $p_\perp$ is the track momentum transverse to the beam axis in GeV/c.

Identification of charged tracks is accomplished with the Cherenkov Ring Imaging

Detector (CRID) [7]. Through the combined use of liquid C_6F_{14} and gaseous C_5F_{12} radiators, it is designed to perform efficient charged $\pi/K/p$ separation over most of the momentum range up to 46 GeV. Charged particles above Cherenkov threshold passing through the radiators emit photons, which are imaged through quartz windows into time projection chambers (TPCs) containing a photosensitive gas. The resulting photoelectrons drift to wire chambers where the conversion point of each is measured in three dimensions using drift time, wire address and charge division. These positions are used to reconstruct a Cherenkov angle with respect to each extrapolated charged track.

The barrel CRID was fully operational for most of the 1993-5 runs and was used in this analysis. The barrel liquid (gas) radiators cover the polar angle range $|\cos\theta| \leq 0.75$ (0.67). The liquid (gas) index of refraction was measured to be 1.282 (1.00165), corresponding to $\pi/K/p$ thresholds of 0.17/0.62/1.17 (2.4/8.6/16.3) GeV/c. The average detected photon yield was 12.5 (9) per full ring for tracks with high velocity. The average Cherenkov angle resolution was 16 (5.5) mrad including the effects of residual misalignments and track extrapolation resolution. The local or intrinsic resolution was 13 (4) mrad, consistent with the design value. The identification performance of the barrel CRID is described in the next section.

The trigger and initial selection of hadronic events is described in [8]. The analysis presented here is based on charged tracks measured in the CDC and VXD. A set of cuts was applied in order to select events well-contained within the detector acceptance. Tracks were required to have (i) a closest approach to the beam axis within 5 cm, and within 10 cm along the beam axis of the measured interaction point (IP), (ii) a polar angle θ with respect to the beam axis with $|\cos\theta| < 0.80$, (iii) a minimum momentum transverse to this axis of $p_\perp > 150$ MeV/c, and (iv) a maximum momentum of $p < 50$ GeV/c. Events were required to contain a minimum of seven such tracks, a thrust [9] axis polar angle with respect to the beam axis θ_T within $|\cos\theta_T| < 0.71$, and a minimum charged visible energy $E_{vis} > 18$ GeV, where all tracks were assigned the charged pion

mass. A sample comprising 100,720 events passed these cuts. Of these, 76,445 events were recorded with a fully operational CRID with a good drift velocity calibration.

Samples enriched in light and b primary flavors were selected based on impact parameters of charged tracks measured in the VXD. We define n_{sig} as the number of tracks in an event with normalized transverse impact parameter with respect to the IP > 3. Events with $n_{sig} = 0$ were assigned to the light flavor sample and those with $n_{sig} \geq 3$ were assigned to the b sample. The light and b samples comprised 60,654 and 14,660 events, respectively, and purities of 86% and 90% were estimated from Monte Carlo simulations. A more detailed discussion of flavor tagging can be found in [10].

Collisions at SLC are produced by highly polarized electron beams. For the 1993 and 1994/5 runs the average beam polarizations were 63% and 77%, respectively, and the beam helicity was selected randomly between collisions. The beam polarization induces a large asymmetry in the polar angle distributions of quark jets, which prefer to follow the electron (positron) beam direction for left- (right-)handed beam. Each event was divided into two hemispheres by the plane perpendicular to the thrust axis $\vec{t}$, and tracks with $\vec{p} \cdot \vec{t} > 0$ were assumed to have come from a jet with polar angle $\theta_h = \cos^{-1}(t_z/|t|)$, where t_z is the component of the thrust axis along the electron beam direction. The remaining tracks were assigned $\theta_h = \cos^{-1}(-t_z/|t|)$. Hemispheres with $\cos \theta_h > 0.2$ produced with left-handed beam and those with $\cos \theta_h < -0.2$ produced with right-handed beam were tagged as quark jets. Hemispheres opposite quark-tagged jets were tagged as antiquark jets. A loose light event tag, requiring $n_{sig} \leq 1$, was also applied. The Standard Model at tree level predicts the purities of the quark- and antiquark-tagged samples to be 70%.

3 Charged Hadron Fractions

The charged π, K and p analysis was performed separately for the liquid and gas radiators. In order to ensure that the CRID performance was well-modelled by the

simulation, tracks were required to traverse an active region of the radiator in question and to have their expected ring fully contained within a live region of the TPCs. The liquid analysis was restricted to the 1993 data sample (22,840 events) and tracks were required to have an associated minimum-ionizing hit in a CRID TPC. For the gas analysis either the minimum-ionizing hit or the presence of at least four hits consistent with a liquid ring was required. For momenta below 2 GeV/c, only negatively charged tracks were used since tracks arising from interactions in the detector material are predominantly positive. In each momentum bin we measured the fractions of the selected tracks of the types π, K and p. Electrons and muons were not distinguished from pions in this analysis; this small background was estimated from the Monte Carlo Simulation (MC) and a correction was applied. The fractions were then multiplied by the total charged hadron spectrum to obtain production cross sections.

Tracks were identified using a likelihood technique. For each of the charged particle hypotheses a likelihood was calculated based upon the number of detected photo-electrons and their measured angles, the expected number of photons, the expected Cherenkov angle and a locally-measured background that included the effects of over-lapping rings. Particle separation was based upon differences between logarithms of these three likelihoods, L_π, L_K and L_p. For the liquid (gas) analysis, we define a particle to be identified as type i if L_i exceeds both of the other log-likelihoods by at least 5 (3), corresponding to 3.2(2.4)σ separation.

The efficiencies for identifying selected particles of type i as type j, where $i, j = \pi, K, p$, are shown in fig. 1. The correct identification rates peak near 90% and the pion coverage is continuous from 0.5 GeV/c up to approximately 25 GeV/c. Misidentification rates in the liquid (gas) are typically less than 3 (5)% with peak values of up to 5 (9)%. These efficiencies were determined through detailed detector simulation and were then calibrated using data. Figure 2 shows the leftmost column of the previous figure measured using a high-purity sample of pions from K^0_s decays in the data and compared with the same analysis of the MC sample. The MC reproduces the data within

6

statistical errors. Simulated efficiencies were parametrized as a function of momentum in order to smooth the effect of limited MC statistics. The form of the parametrization of the simulated $\pi \rightarrow \pi$ efficiency provides a good fit to the efficiencies extracted using K_s^0 decays, and fitted parameter values for MC and data K_s^0 are consistent. For the liquid analysis the parametrized MC was therefore used to define the central values of the efficiencies. For correct identification the statistical errors on parameter values from the fit to the K_s^0 data were used to define the errors on the efficiencies, which are shown in fig. 1 and are correlated point to point. For misidentification a common relative error of 0.16 was assumed, corresponding to one-half of a typical statistical error on the K_s^0 data points. For misidentification in the gas the MC was also used for the central values and a common relative error of 0.25 was assigned. The limited size of the K_s^0 data sample does not provide a strong constraint on efficiencies in the gas analysis, so the total rates of identification as any hadron type in the data and MC were compared. This resulted in a correction of -1.3% to the $\pi \rightarrow \pi$ efficiencies in the threshold region, $3 < p < 10.5$ GeV/c, and -3% to all identification efficiencies above 10.5 GeV/c. The larger of the correction itself or the statistical error on the total rate in the data was taken as the error on each point and these errors are strongly positively correlated.

For each momentum bin the number of observed particles of a given type can be related to the true production fraction by an efficiency matrix, composed of the entries in fig. 1 for that bin. This matrix was inverted and used to unfold our observed identified particle rates. This analysis procedure does not require that the sum of the charged particle fractions be unity; instead the sum was used as a consistency check and was found to be in good agreement with unity for all momenta.

The measured charged particle fractions for hadronic Z^0 decays are shown in fig. 3. In some momentum regions we cannot distinguish two of the three species, so the procedure was reduced to a 2×2 analysis and we present only the fraction of the iden- tified species, i.e. protons in the liquid (gas) analysis above 3 (27) GeV/c and pions

in the gas analysis below 10.5 GeV/c. The errors on the liquid points are dominated by systematics which are strongly positively correlated point to point and increase in magnitude with momentum. The errors on the gas points have roughly equal statistical and systematic contributions, with similar systematic correlation. Pions are seen to dominate the particle production at low momentum, to decline steadily until about 10 GeV/c, and to level off at about two-thirds. The kaon fraction rises steadily to about one-third at high momentum. The proton fraction rises at low momentum, levels off near one-tenth at about 10 GeV/c, then declines above 25 GeV/c. Where the momentum coverage overlaps, these measured fractions were found to be in agreement with previous measurements at the Z^0 [3, 11, 12]. Measurements based on ring imaging and those based on ionization energy loss rates [11, 12] cover complementary momentum ranges and can be combined to provide continuous coverage from 200 MeV/c to 35 GeV/c.

4 Neutral V^0 Production

To measure the production of $\Lambda^0/\bar{\Lambda}^0$ and K^0, all pairs of oppositely-charged tracks were considered as "V^0" candidates if both tracks had (i) at least 40 hits in the CDC, (ii) $|\cos\theta| < 0.80$ and (iii) $p_\perp > 150$ MeV/c. A vertex was fitted to each pair and the probability of the resulting χ^2 was required to be greater than 2%. The vertex was required to be displaced from the IP by at least 5 standard deviations, which accepted V^0 candidates with flight lengths as low as 0.2 mm. The angle α_{xy} between the V^0 momentum and the vector from the IP to the vertex in the transverse plane was required to satisfy $|\alpha_{xy}| < 5 + 50/p_\perp + 12.5/p_\perp^2$ mrad, where $p_\perp$ is the momentum of the V^0 candidate transverse to the beam axis. Candidates were rejected if their vertex was located outside of the VXD but included a track with more than one VXD hit.

Photon conversions were suppressed by requiring the e^+e^- invariant mass of the charged track pair to be greater than 70 MeV/c^2. Kinematically-overlapped K^0_s were

rejected from the Λ^0 sample by rejecting all pairs whose $\pi\pi$ invariant mass was within 3σ of the K_s^0 mass, which removed approximately 30% of the Λ^0 sample. Λ^0 were removed from the K_s^0 sample by requiring $|\cos\theta^*| < 0.8$, where θ^* is the angle between the positively charged track and the V^0 flight direction in the $\pi^+\pi^-$ rest frame, resulting in a 20% loss of the K_s^0 signal.

The remaining V^0 candidates were divided into bins in both scaled momentum $x_p = 2p/W$ and $\xi = \ln(W/2p)$. In each bin the numbers of observed K_s^0 and Λ^0 were derived from the $\pi\pi$ and $p\pi$ invariant mass distributions, respectively, where the faster track was assigned the proton mass. These numbers were divided by reconstruction efficiencies estimated from MC to yield production spectra. The reconstruction efficiencies are shown as a function of ξ in fig. 4. As a check the K_s^0 and Λ^0 lifetimes were measured to be $c\tau_{K_S^0} = 2.59 \pm 0.07$ and $c\tau_{\Lambda^0} = 7.25 \pm 0.38(\text{stat.})$ cm in agreement with world average values [13].

5 Results

Figure 5 shows the production cross sections as a function of scaled momentum $x_p = 2p/W$ for the five measured species. For the charged species, cross-sections were obtained by multiplying the measured fractions by the total hadronic cross-section generated by the JETSET 7.4 simulation program, which provides a good description of data at the Z^0 [14]. The cross sections for charged and neutral kaon production are consistent. Table 1 shows the total production rate per event of each species over the momentum range which we measure. The errors are dominated by overall normalization uncertainties.

For comparison with QCD+LPHD predictions the analysis was repeated as a function of $\xi = \ln(1/x_p)$. The resulting spectra are shown in fig. 6 and were fitted using Gaussian approximations to the prediction [1]. This shape describes the data adequately within our point-to-point errors. For the neutrals and the charged pions the

data cover the peak well and Table 2 lists the peak positions ζ^* obtained from these fits. The systematic error is due to variation of the fit range and, in the case of the charged pions, the difference between a fit to the liquid points only and a fit in which the liquid points were deweighted by a factor of 5. We note that fits to the charged kaon and proton spectra give results similar to the neutral kaons and lambdas, respectively.

The pions peak at higher ζ (lower momentum) than the other particles, as predicted by QCD+LPHD; however, we do not see a substantial peak shift between the kaons and the baryons. These results are in agreement with previous measurements [3].

Particle	Momentum Range (GeV/c)	Production Rates per Hadronic Event
$\pi^\pm$	0.7–27	11.12±0.35
$K^\pm$	0.75–3	0.74±0.09
$K^\pm$	10.5–27	0.19±0.02
$p/\bar{p}$	1.25–5.5	0.48±0.05
$p/\bar{p}$	10.5–36	0.07±0.01
K^0	0.5–13.7	1.75±0.07
$\Lambda^0/\bar{\Lambda}^0$	0.5–13.7	0.34±0.02

Table 1: Preliminary production rates of identified particles in hadronic Z^0 decays. The errors are dominated by overall systematic errors.

Particle	ζ-Peak Position
$\pi^\pm$	3.74±0.01±0.04
K^0	2.60±0.02±0.02
$\Lambda^0/\bar{\Lambda}^0$	2.63±0.04±0.01

Table 2: Preliminary spectrum peak positions (ζ^*) for charged pions and neutral kaons and lambdas.

The analysis was repeated on the high-purity light- and b-quark samples described in section 2. The measured cross sections for these two samples are shown in fig. 7.

There is higher production of both charged and neutral kaons and charged pions in the b-tagged sample than in the light-tagged sample, and lower production of baryons. The spectra of all species are found to fall more rapidly at low ξ in the b-tagged sample, and those of the mesons also fall more rapidly at high ξ. For the charged pions there is a difference in fitted peak position of 0.15 ± 0.05 between the light and b-tagged samples. We do not observe significant differences in peak position for the other species. The charged hadron fractions for these two samples (not shown) are quite similar, with the b sample showing a few percent lower pion fraction in the range $3 < p < 10$ GeV/c, a higher pion fraction above 15 GeV/c and a lower proton fraction above 15 GeV/c.

The charged fractions analysis was repeated separately on the positively- and negatively-charged tracks in the quark-tagged sample described in section 2. The V^0 analysis was repeated separately on candidates with the positively- and negatively-charged track assigned the proton mass. Tracks and V^0s in the antiquark-tagged sample were included but with their charges reversed. Figure 8 shows the differences between the baryon and antibaryon production spectra normalized by their averages, $d_X = 2(n_X - n_{\overline{X}})/(n_X + n_{\overline{X}})$, $X = p, \Lambda^0$, as a function of scaled momentum. At low momentum they are consistent with zero, corresponding to equal production of baryons and antibaryons. The differences are predominantly positive above about 12 GeV/c, corresponding to an excess of baryon production, and suggest an upward trend with momentum. MC studies and the above measurements in the b-sample indicate that contributions to the baryon and antibaryon samples from heavy hadron decays are much smaller than the observed differences at high momentum. These differences therefore provide direct evidence that faster particles are more likely to contain the initial quark.

6 Summary and Conclusions

Using the SLD CRID we have made preliminary measurements of charged pion, kaon and proton production over a large momentum range in hadronic Z^0 decays, complementing previous measurements based on ionization energy loss. The production of K^0 and $\Lambda^0/\bar{\Lambda}^0$ was also studied. Spectrum shapes were found to be adequately described by the Gaussian approximation to the QCD+LPHD prediction. Our results for the global sample are in agreement with previous measurements. By isolating high-purity light- and b-quark samples it was shown that spectrum shapes are affected by heavy

quark fragmentation and decay, but that the effect on the ξ-peak positions is small. We observed a difference in spectra at high momentum between baryons and antibaryons in a high-purity sample of quark jets, providing direct evidence that particles containing a primary quark have a harder fragmentation spectrum than those that do not.

Acknowledgements

References

[1] T.I. Azimov, Y.L. Dokshitzer, V.A. Khoze and S.I. Troyan, Z. Phys. **C27** (1985) 65.

[2] See e.g. A. DeAngelis, CERN-PPE/90-129.

[3] DELPHI Collab., P. Abreu *et al.*, CERN-PPE-95/28, submitted to Nucl. Phys. B.

[4] SLD Design Report, SLAC-REPORT 273, (1984).

[5] M.D. Hildreth *et al.*, SLAC-PUB-6656 (1994), submitted to IEEE Trans. Nucl. Sci.

[6] C. J. S. Damerell *et al.*, Nucl. Inst. Meth. **A288** (1990) 288.

[7] K. Abe, *et al.*, Nucl. Inst. Meth. **A343** (1994) 74.

[8] SLD Collab., K. Abe *et al.*, Phys. Rev. Lett. **73** (1994) 25.

[9] S. Brandt *et al.*, Phys. Lett. **12** (1964) 57.
E. Farhi, Phys. Rev. Lett. **39** (1977) 1587.

[10] SLD Collab., K. Abe *et al.*, SLAC-PUB-95-6921, "Measurement of the Charged Multiplicities of b, c and Light Quark Events from Z^0 Decays", contributed to this conference; SLAC-PUB-6589 submitted to Phys. Rev. D.

[11] OPAL Collab., P.D. Acton *et al.*, *Z. Phys.* **C63** (1994) 181.

[12] ALEPH Collab., D. Decamp *et al.*, CERN-PPE-94/201, submitted to Z. Phys. C.

[13] Particle Data Group, Phys. Rev. **D50** (1994) 1173.

[14] ALEPH Collab., D. Decamp *et al.*, Z. Phys. **C55** (1992) 209.

List of Authors

.. K. Abe,[29] I. Abt,[14] C.J. Ahn,[26] T. Akagi,[27] N.J. Allen,[4] W.W. Ash,[27]†
D. Aston,[27] K.G. Baird,[24] C. Baltay,[33] H.R. Band,[32] M.B. Barakat,[33]
G. Baranko,[10] O. Bardon,[16] T. Barklow,[27] A.O. Bazarko,[11] R. Ben-David,[33]
A.C. Benvenuti,[2] T. Bienz,[27] G.M. Bilei,[22] D. Bisello,[21] G. Blaylock,[7]
J.R. Bogart,[27] T. Bolton,[11] G.R. Bower,[27] J.E. Brau,[20] M. Breidenbach,[27]
W.M. Bugg,[28] D. Burke,[27] T.H. Burnett,[31] P.N. Burrows,[16] W. Busza,[16]
A. Calcaterra,[13] D.O. Caldwell,[6] D. Calloway,[27] B. Camanzi,[12] M. Carpinelli,[23]
R. Cassell,[27] R. Castaldi,[23](a) A. Castro,[21] M. Cavalli-Sforza,[7] E. Church,[31]
H.O. Cohn,[28] J.A. Coller,[3] V. Cook,[31] R. Cotton,[4] R.F. Cowan,[16]
D.G. Coyne,[7] A. D'Oliveira,[8] C.J.S. Damerell,[25] M. Daoudi,[27] R. De Sangro,[13]
P. De Simone,[13] R. Dell'Orso,[23] M. Dima,[9] P.Y.C. Du,[28] R. Dubois,[27]
B.I. Eisenstein,[14] R. Elia,[27] D. Falciai,[22] M.J. Fero,[16] R. Frey,[20] K. Furuno,[20]
T. Gillman,[25] G. Gladding,[14] S. Gonzalez,[16] G.D. Hallewell,[27] E.L. Hart,[28]
Y. Hasegawa,[29] S. Hedges,[4] S.S. Hertzbach,[17] M.D. Hildreth,[27] J. Huber,[20]
M.E. Huffer,[27] E.W. Hughes,[27] H. Hwang,[20] Y. Iwasaki,[29] D.J. Jackson,[25]
P. Jacques,[24] J. Jaros,[27] A.S. Johnson,[3] J.R. Johnson,[32] R.A. Johnson,[8]
T. Junk,[27] R. Kajikawa,[19] M. Kalelkar,[24] H. J. Kang,[26] I. Karliner,[14]
H. Kawahara,[27] H.W. Kendall,[16] Y. Kim,[26] M.E. King,[27] R. King,[27]
R.R. Kofler,[17] N.M. Krishna,[10] R.S. Kroeger,[18] J.F. Labs,[27] M. Langston,[20]
A. Lath,[16] J.A. Lauber,[10] D.W.G. Leith,[27] M.X. Liu,[33] X. Liu,[7] M. Loreti,[21]
A. Lu,[6] H.L. Lynch,[27] J. Ma,[31] G. Mancinelli,[22] S. Manly,[33] G. Mantovani,[22]
T.W. Markiewicz,[27] T. Maruyama,[27] R. Massetti,[22] H. Masuda,[27]
T.S. Mattison,[27] E. Mazzucato,[12] A.K. McKemey,[4] B.T. Meadows,[8]
R. Messner,[27] P.M. Mockett,[31] K.C. Moffeit,[27] B. Mours,[27] G. Müller,[27]
D. Muller,[27] T. Nagamine,[27] U. Nauenberg,[10] H. Neal,[27] M. Nussbaum,[8]
Y. Ohnishi,[19] L.S. Osborne,[16] R.S. Panvini,[30] H. Park,[20] T.J. Pavel,[27]
I. Peruzzi,[13](b) M. Piccolo,[13] L. Piemontese,[12] E. Pieroni,[23] K.T. Pitts,[20]
R.J. Plano,[24] R. Prepost,[32] C.Y. Prescott,[27] G.D. Punkar,[27] J. Quigley,[16]
B.N. Ratcliff,[27] T.W. Reeves,[30] J. Reidy,[18] P.E. Rensing,[27] L.S. Rochester,[27]
J.E. Rothberg,[31] P.C. Rowson,[11] J.J. Russell,[27] O.H. Saxton,[27]
S.F. Schaffner,[27] T. Schalk,[7] R.H. Schindler,[27] U. Schneekloth,[16]
B.A. Schumm,[15] A. Seiden,[7] S. Sen,[33] V.V. Serbo,[32] M.H. Shaevitz,[11]
J.T. Shank,[3] G. Shapiro,[15] S.L. Shapiro,[27] D.J. Sherden,[27] K.D. Shmakov,[28]
C. Simopoulos,[27] N.B. Sinev,[20] S.R. Smith,[27] J.A. Snyder,[33] P. Stamer,[24]
H. Steiner,[15] R. Steiner,[1] M.G. Strauss,[17] D. Su,[27] F. Suekane,[29]
A. Sugiyama,[19] S. Suzuki,[19] M. Swartz,[27] A. Szumilo,[31] T. Takahashi,[27]
F.E. Taylor,[16] E. Torrence,[16] J.D. Turk,[33] T. Usher,[27] J. Va'vra,[27]
C. Vannini,[23] E. Vella,[27] J.P. Venuti,[30] R. Verdier,[16] P.G. Verdini,[23]
S.R. Wagner,[27] A.P. Waite,[27] S.J. Watts,[4] A.W. Weidemann,[28] E.R. Weiss,[31]
J.S. Whitaker,[3] S.L. White,[28] F.J. Wickens,[25] D.A. Williams,[7]
D.C. Williams,[16] S.H. Williams,[27] S. Willocq,[33] R.J. Wilson,[9]
W.J. Wisniewski,[5] M. Woods,[27] G.B. Word,[24] J. Wyss,[21] R.K. Yamamoto,[16]
J.M. Yamartino,[16] X. Yang,[20] S.J. Yellin,[6] C.C. Young,[27] H. Yuta,[29]

G. Zapalac,[32] R.W. Zdarko,[27] C. Zeitlin,[20] Z. Zhang,[16] and J. Zhou,[20]

[1]*Adelphi University, Garden City, New York 11530*
[2]*INFN Sezione di Bologna, I-40126 Bologna, Italy*
[3]*Boston University, Boston, Massachusetts 02215*
[4]*Brunel University, Uxbridge, Middlesex UB8 3PH, United Kingdom*
[5]*California Institute of Technology, Pasadena, California 91125*
[6]*University of California at Santa Barbara, Santa Barbara, California 93106*
[7]*University of California at Santa Cruz, Santa Cruz, California 95064*
[8]*University of Cincinnati, Cincinnati, Ohio 45221*
[9]*Colorado State University, Fort Collins, Colorado 80523*
[10]*University of Colorado, Boulder, Colorado 80309*
[11]*Columbia University, New York, New York 10027*
[12]*INFN Sezione di Ferrara and Università di Ferrara, I-44100 Ferrara, Italy*
[13]*INFN Lab. Nazionali di Frascati, I-00044 Frascati, Italy*
[14]*University of Illinois, Urbana, Illinois 61801*
[15]*Lawrence Berkeley Laboratory, University of California, Berkeley, California 94720*
[16]*Massachusetts Institute of Technology, Cambridge, Massachusetts 02139*
[17]*University of Massachusetts, Amherst, Massachusetts 01003*
[18]*University of Mississippi, University, Mississippi 38677*
[19]*Nagoya University, Chikusa-ku, Nagoya 464 Japan*
[20]*University of Oregon, Eugene, Oregon 97403*
[21]*INFN Sezione di Padova and Università di Padova, I-35100 Padova, Italy*
[22]*INFN Sezione di Perugia and Università di Perugia, I-06100 Perugia, Italy*
[23]*INFN Sezione di Pisa and Università di Pisa, I-56100 Pisa, Italy*
[24]*Rutgers University, Piscataway, New Jersey 08855*
[25]*Rutherford Appleton Laboratory, Chilton, Didcot, Oxon OX11 0QX United Kingdom*
[26]*Sogang University, Seoul, Korea*
[27]*Stanford Linear Accelerator Center, Stanford University, Stanford, California 94309*
[28]*University of Tennessee, Knoxville, Tennessee 37996*
[29]*Tohoku University, Sendai 980 Japan*
[30]*Vanderbilt University, Nashville, Tennessee 37235*
[31]*University of Washington, Seattle, Washington 98195*
[32]*University of Wisconsin, Madison, Wisconsin 53706*
[33]*Yale University, New Haven, Connecticut 06511*
†*Deceased*
[a]*Also at the Università di Genova*
[b]*Also at the Università di Perugia*

Figure captions

1. Identification efficiencies for charged $\pi^{\pm}$, $K^{\pm}$, and $p/\bar{p}$ in the SLD barrel CRID, with systematic errors. The open symbols are for the analysis using liquid radiator information; the solid symbols are for the gaseous radiator.

2. Identification efficiencies for charged $\pi^{\pm}$ measured with pions from K_s^0 decays (solid symbols). The open circles are for the same analysis of a Monte Carlo sample.

3. Preliminary charged hadron fractions measured by SLD. Circles are $\pi^{\pm}$, squares are $K^{\pm}$, and triangles are $p/\bar{p}$. Open symbols are for the liquid radiator; solid symbols are for the gas.

4. The efficiency for reconstructing and selecting a) K^0 and b) Λ^0 decays in selected hadronic Z^0 decays recorded by SLD. The efficiencies include the branching ratios and effects of detector acceptance.

5. Preliminary production spectra per event vs. scaled momentum $x_p = 2p/W$ for $\pi^{\pm}$ (dots), $K^{\pm}$ (squares), K^0 (open squares), $p/\bar{p}$ (triangles), and $\Lambda^0/\bar{\Lambda}^0$ (open triangles) in inclusive hadronic Z^0 decays. The $p/\bar{p}$ and $\Lambda^0/\bar{\Lambda}^0$ spectra have been scaled by 0.2 and 0.1, respectively. The errors are statistical and systematic in quadrature. The systematic errors on the charged species are dominant and are correlated point to point. An overall normalization uncertainty of 4% on the neutral species is not included.

6. Preliminary production spectra per event vs. $\xi = -\ln(x_p)$ for a) $\pi^{\pm}$, b) $K^{\pm}$, c) K^0, d) $p/\bar{p}$, and e) $\Lambda^0/\bar{\Lambda}^0$ in inclusive hadronic Z^0 decays. The errors are described in the caption for fig. 5. The curves are results of Gaussian fits.

7. Preliminary production spectra per event vs. $\xi = -\ln(x_p)$ for a) $\pi^{\pm}$, b) $K^{\pm}$, c) K^0, d) $p/\bar{p}$, and e) $\Lambda^0/\bar{\Lambda}^0$ in samples enriched in $Z^0 \rightarrow u\bar{u}, d\bar{d}, s\bar{s}$ decays (solid symbols) and $Z^0 \rightarrow b\bar{b}$ decays (open symbols). Only statistical errors are shown.

8. The difference between p and $\bar{p}$ (circles) and Λ^0 and $\bar{\Lambda}^0$ (squares) production spectra in quark-tagged jets, normalized by their average in each bin. Only statistical errors are shown.

Figure 1:   SLD CRID Identification Efficiencies
(Preliminary)
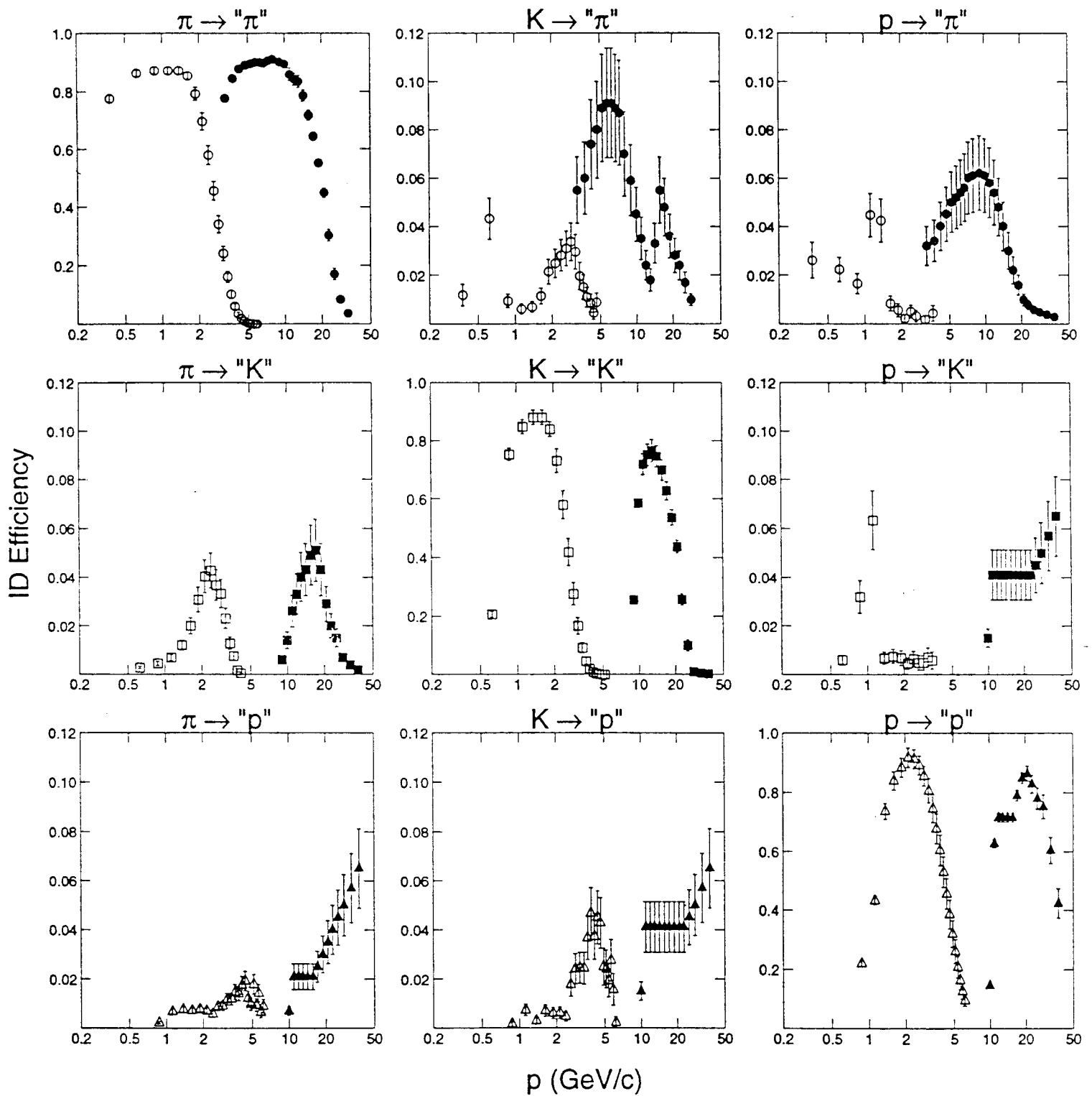
Figure 2: Determination of Liquid ID Efficiencies
using $K_s^0 \rightarrow \pi\pi$
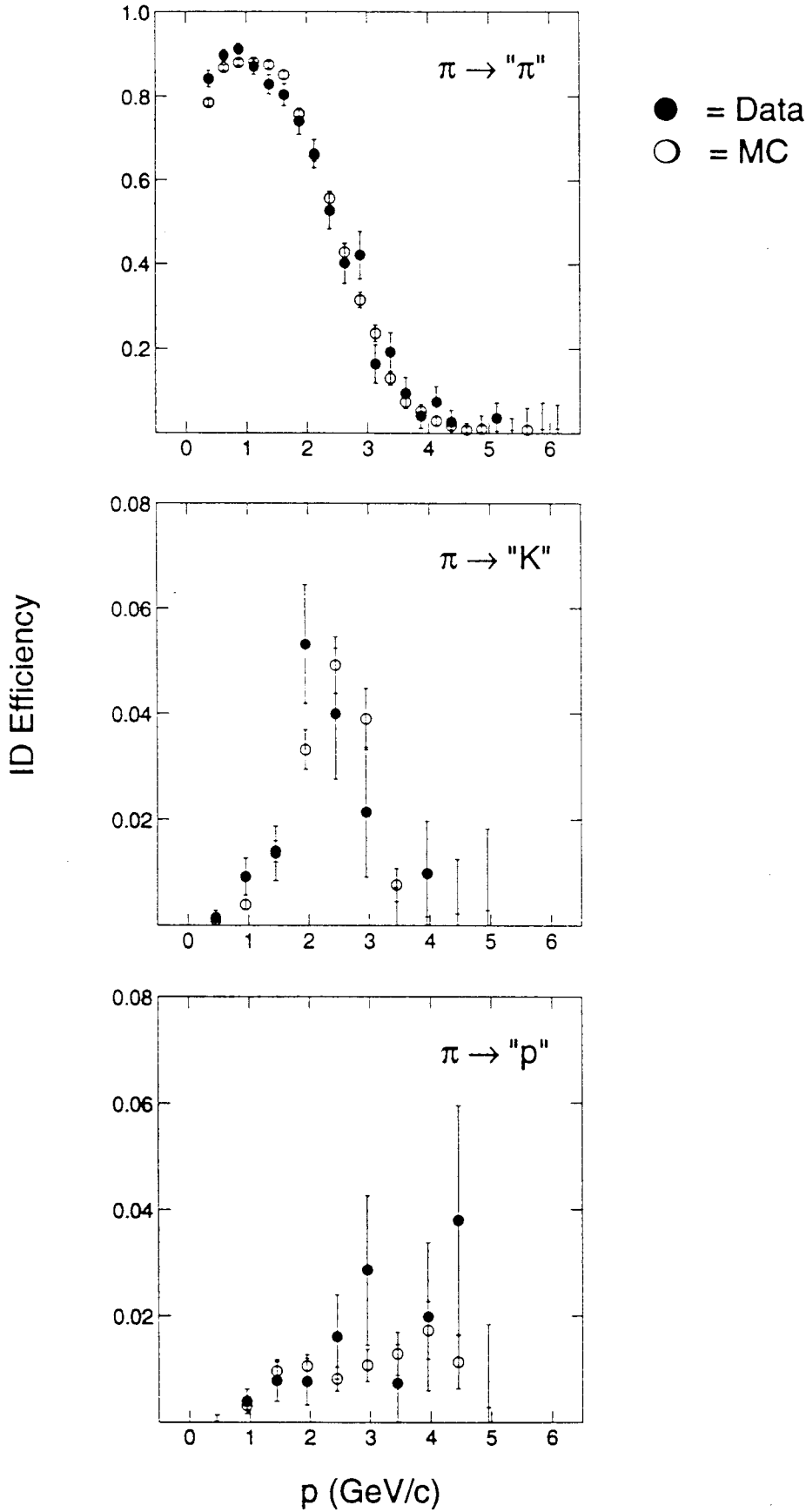
Figure 3: SLD Preliminary Fractions
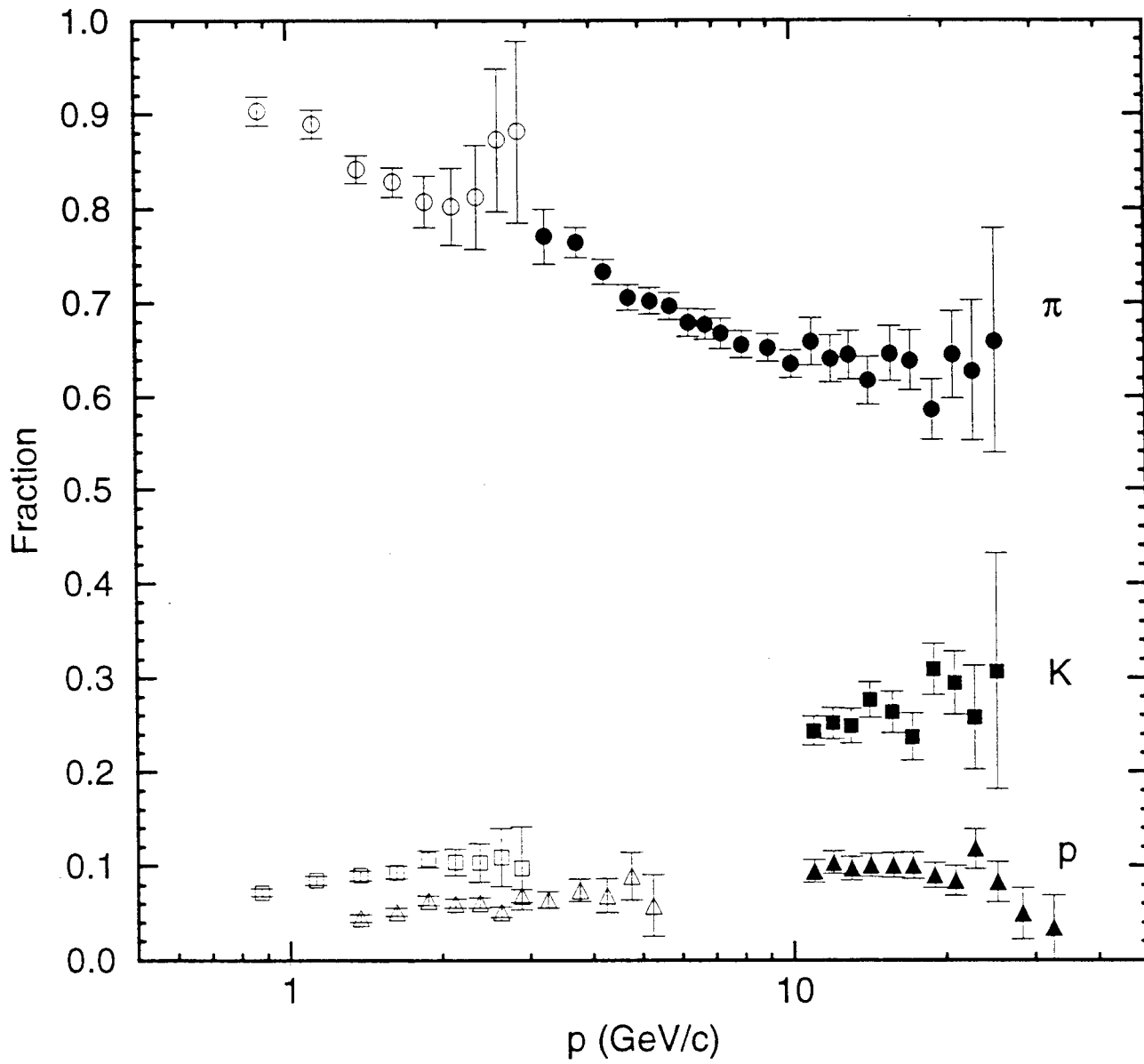
Figure 4: V^0 Reconstruction Efficiencies (Preliminary)
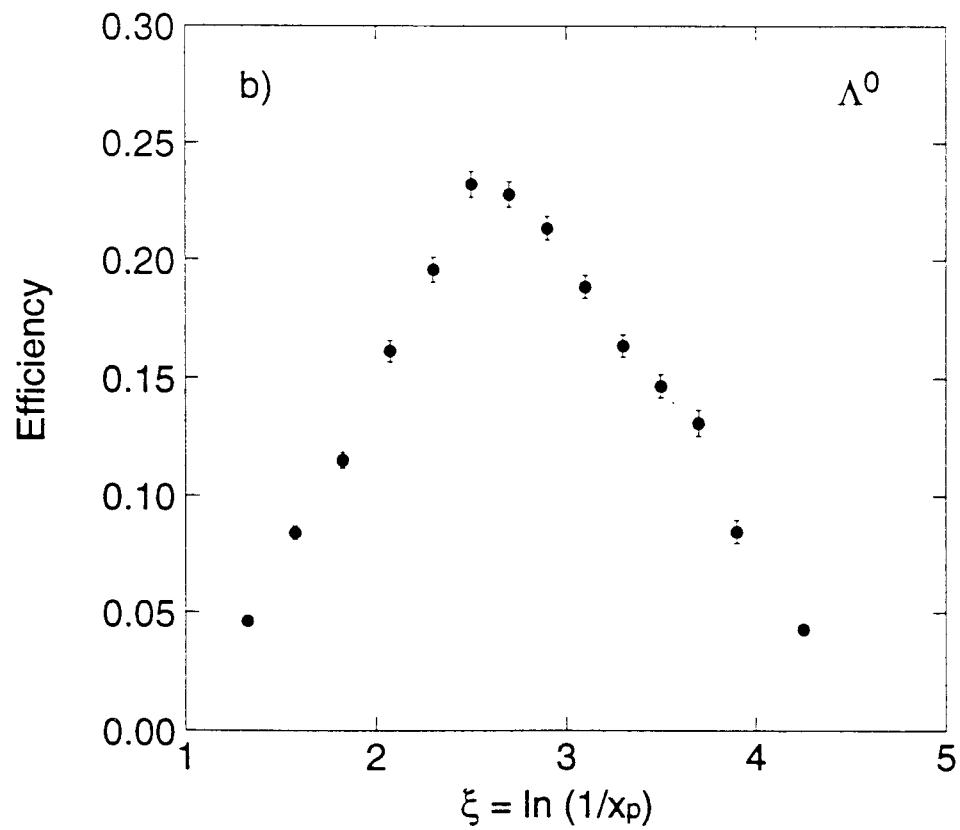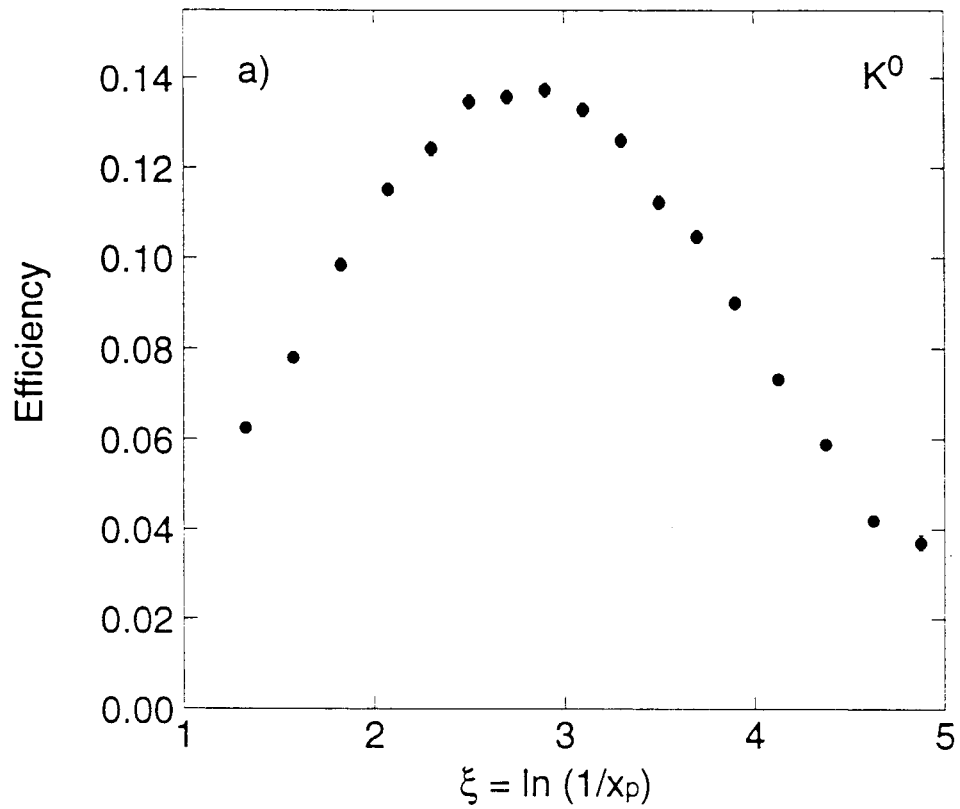
Figure 5: SLD Preliminary Spectra
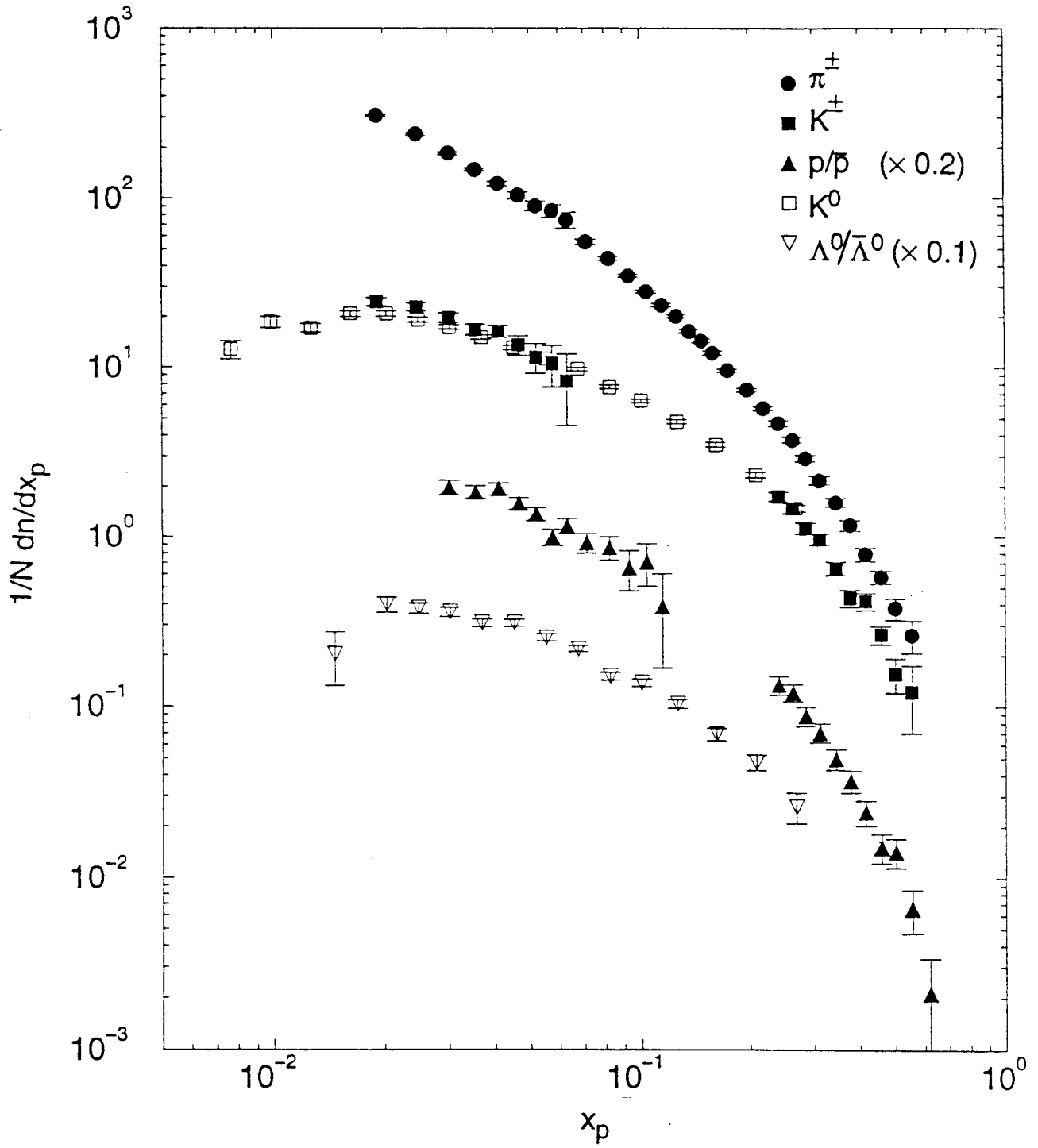
Figure 6: SLD Preliminary Production Spectra

Figure 7: SLD Preliminary uds- and b-Tagged Spectra
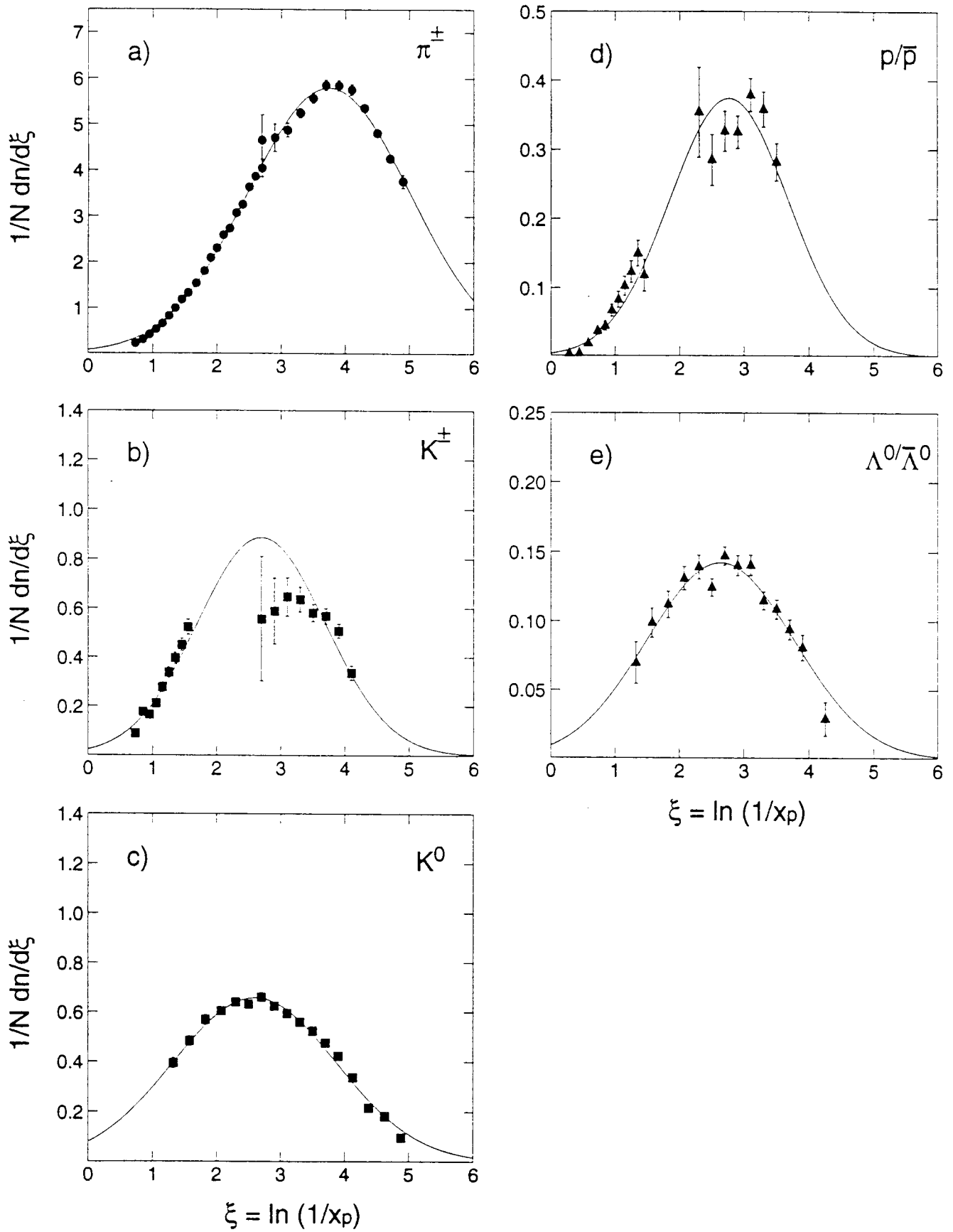
Figure 7: SLD Preliminary uds- and b-Tagged Spectra
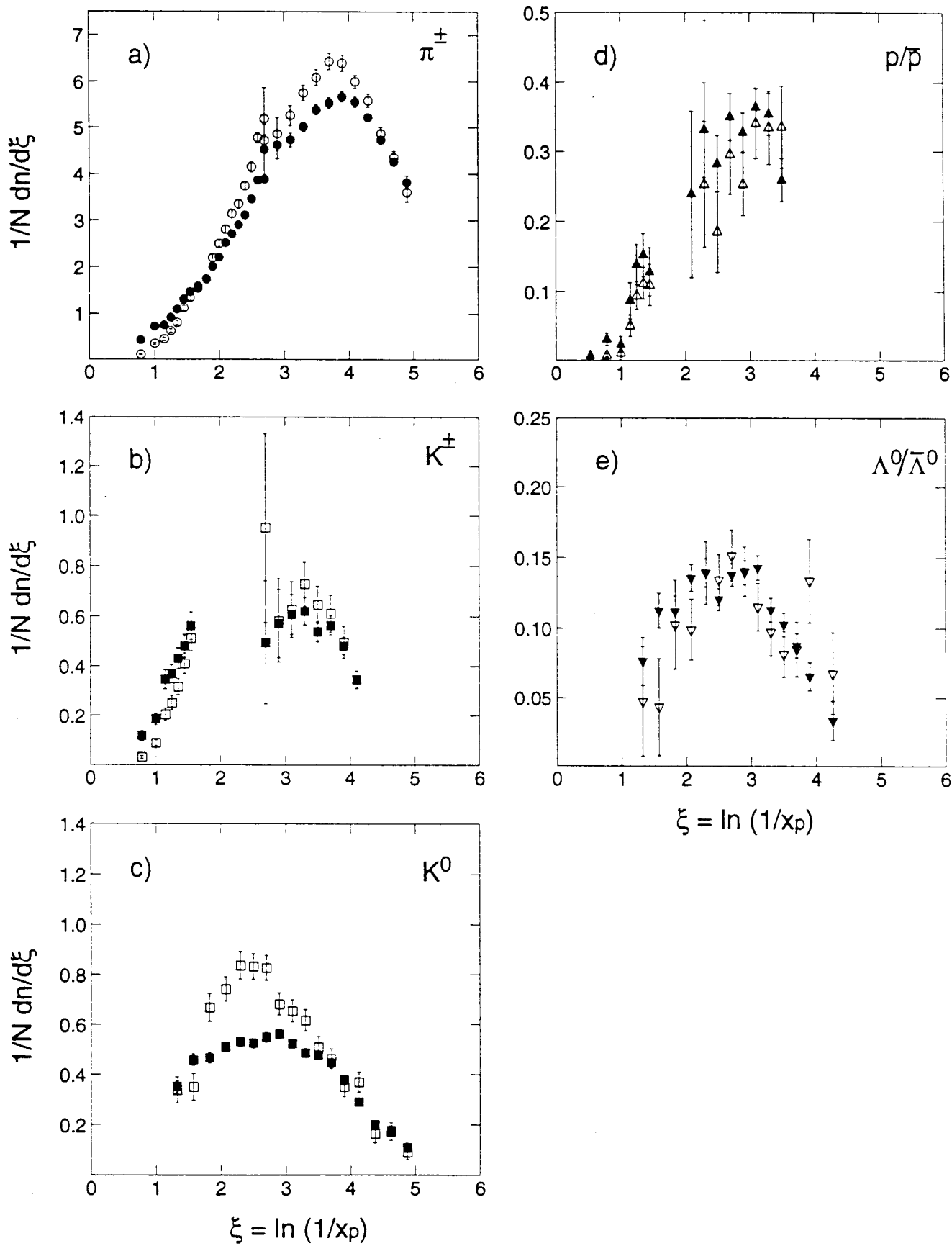
Figure 8: Comparison of baryon and antibaryon production in quark jets